Supporting Information for

A combined experimental and multiscale modeling approach for the investigation of lab-scale fluidized bed reactors

Riccardo Uglietti,[ab‡] Daniele Micale,[a‡] Damiano La Zara,[b] Aris Goulas,[b] Luca Nardi,[a]

Mauro Bracconi,[a] J. Ruud van Ommen,*[b] and Matteo Maestri*[a]

[a] *Laboratory of Catalysis and Catalytic Processes, Dipartimento di Energia, Politecnico di Milano, via La Masa 34, 20156 Milano, Italy.*

[b] *Department of Chemical Engineering, Delft University of Technology, Van der Maasweg 9, 2629 HZ Delft, The Netherlands.*

*to whom correspondence should be addressed:

matteo.maestri@polimi.it (M. Maestri)
J.R.vanOmmen@tudelft.nl (J.R. van Ommen)

1 Particle size distribution

Figure I reports the diameter distribution of the alumina particles, measured by means of the Beckman Coulter laser diffraction particle analyzer.

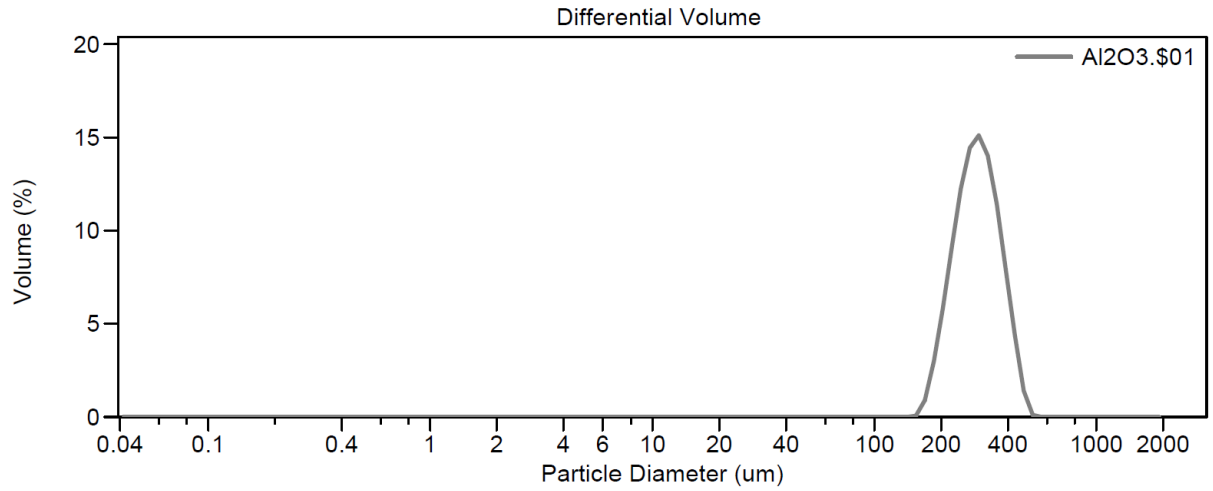

Figure I. *Distribution of the alumina particles diameters measured with the laser diffraction particle analyzer*

A unimodal distribution has been measured, characterized by the following parameters:

- mean particle diameter: 296.2 μm;
- standard deviation: 66.56 μm;
- skewness: 0.419 (right skewed);
- kurtosis: -0.333 (platykurtic);

2 Reactive CFD-DEM Multiscale Framework

The fluidized bed is updated at each time step by solving sequentially the solid and the gas phases in the reactor.

2.1 Solid Phase

The solid phase is updated particle-wise considering the gas phase frozen. Each pellet composing the fluidized bed is tracked through the computational grid, which is fixed and particle-independent. The particle tracking is performed by solving the momentum (Eq. (I)) and angular momentum (Eq. (II)) balances on the catalytic pellet.

$$\frac{d\boldsymbol{v}_p}{dt} = \frac{\boldsymbol{F}_{d,p} + \boldsymbol{F}_{b,p} + \boldsymbol{F}_{coll,p}}{m_p} + \boldsymbol{g} \tag{I}$$

$$\frac{d\boldsymbol{w}_p}{dt} = \frac{\sum[R_p \boldsymbol{n} \wedge \boldsymbol{F}_{coll,p}]}{I_p} \tag{II}$$

where m, I, **v**, **w** are the mass, the moment of inertia, the velocity and angular velocity of the p^{th} particle, $\boldsymbol{F}_{coll,p}$ is the total collision force acting on the particle p, $\boldsymbol{F}_{d,p}$ is the drag force between the gas and the particle p, $\boldsymbol{F}_{b,p}$ is the buoyancy force, **n** is the unit normal to the direction of the total collisional force and R_p is the particle p radius.

The total collisional force acting on the generic particle p is computed by means of a soft-sphere approach[1]. According to this method, the collisions involving p^{th} particle during a time step are first detected whenever particle p is overlapped with another one. Then, the collision force is computed for each detected collisional event as a function of the relative velocity and the magnitude of the overlap vector by means of a spring-slider-dashpot model[2] (Eqs. (III)-(IV)).

$$\boldsymbol{F}_{ab,n} = \left(-k_n \delta_n^{\frac{3}{2}} - \eta_n \boldsymbol{v}_{ab} \cdot \boldsymbol{n}_{ab}\right) \boldsymbol{n}_{ab} \tag{III}$$

$$\boldsymbol{F}_{ab,t} = \begin{cases} \left(\mu_c \left\|\boldsymbol{F}_{ab,n}\right\|\right) \boldsymbol{t}_{ab} & \left\|\boldsymbol{F}_{ab,t}\right\| > \mu_c \left\|\boldsymbol{F}_{ab,n}\right\| \\ -k_t \delta_t \boldsymbol{t}_{ab} - \eta_t (\boldsymbol{v}_{ab} - (\boldsymbol{v}_{ab} \cdot \boldsymbol{n}_{ab}) \boldsymbol{n}_{ab} & \left\|\boldsymbol{F}_{ab,t}\right\| \leq \mu_c \left\|\boldsymbol{F}_{ab,n}\right\| \end{cases} \tag{IV}$$

where $\boldsymbol{v}_{ab}$ is the relative velocity between the two colliding particles a and b, $\boldsymbol{n}_{ab}$ is the unit vector connecting the centers of a and b, $\boldsymbol{t}_{ab}$ is the tangential unit vector normal to $\boldsymbol{n}_{ab}$, μ_c is the friction factor of the slider and k and η are the spring stiffness and the damping coefficient of the dashpot which can be derived from the Young modulus E, the Poisson ratio ν and the restitution coefficient e of the particles as proposed by Tsuji at al.[2]. Subscripts n and t refer to the normal and tangential directions with respect to the plane normal to $\boldsymbol{n}_{ab}$. Finally, each collisional force vector is summed up to obtain the total force vector acting on particle p at that specific time step.

The drag force (Eq. (V)) is a function of a drag coefficient β computed by means of the Gidaspow model[3] (Eq. (VI)) and the relative velocity vector. In particular, the drag coefficient is a function of the magnitude of the relative velocity vector, the geometry of the particle and the gas fraction in the computational cell hosting the particle (ε_g), which is computed by means a Particle Centroid Method – PCM[4].

$$\boldsymbol{F}_{d,p} = V_p \beta \left(\boldsymbol{U}_g - \boldsymbol{v}_p \right) \tag{V}$$

$$\beta = \begin{cases} \dfrac{150(1-\varepsilon_g)}{\varepsilon_g} \dfrac{\mu_g}{D_p^2} + 1.75\left(1-\varepsilon_g\right) \dfrac{\rho_g}{D_p} \left\| \boldsymbol{U}_g - \boldsymbol{v}_p \right\| & \epsilon < 0.8 \\ \dfrac{3}{4} C_D \dfrac{\rho_g}{D_p} \left\| \boldsymbol{U}_g - \boldsymbol{v}_p \right\| {\varepsilon_g}^{-1.65} & \epsilon \geq 0.8 \end{cases} \tag{VI}$$

where μ_g is the gas dynamic viscosity, D_p is the particle diameter, V_p is the volume of the particle, ρ_g is the density of the gas phase at the particle position, $\boldsymbol{U}_g - \boldsymbol{v}_p$ is the relative velocity between a generic particle p and the gas phase and C_D is evaluated according to Schiller and Naumann[5] (Eq. (VII)):

$$C_D = \begin{cases} 24[1 + 0.15\left(\varepsilon_g Re_p\right)^{0.687}]/(\varepsilon_g Re_p) & Re_p < 1000 \\ 0.44 & Re_p \geq 1000 \end{cases} \tag{VII}$$

where Re_p is the particle Reynolds number based on the magnitude of the particle-gas relative velocity vector.

The buoyancy force (Eq. (VIII)) is computed as a function of the pressure gradient experienced by the gas surrounding the particle.

$$\boldsymbol{F}_{buoyancy} = V_p \nabla P \tag{VIII}$$

In addition to the particle tracking, the ODE system, composed by the species mass (Eq. (IX)) and site species (Eq. (X)) balances, is integrated for each catalytic pellet.

$$\rho_{g,p} \varepsilon_p \frac{d\omega_{j,p}}{dt} = K_{c,j} S_{v,p} \rho \left(\omega_{j,g} - \omega_{j,p} \right) + \sum_{n=1}^{NR} \nu_{j,n} r_{n,p} MW_j \tag{IX}$$

$$\frac{d\theta_{j,p}}{dt} = \frac{R_{j,p}^{het}}{\sigma_{cat}} \tag{X}$$

where ω_j, $K_{c,j}$, MW_j and $\nu_{j,n}$ are the mass fraction, the mass transfer coefficient, the molecular weight and the stoichiometry coefficient of the nth reaction of the j^{th} species, ε_p is the porosity of the catalyst, $\rho_{g,p}$ is the average density of the perfect gas mixture in the catalyst and ρ is the mean density between the mixture in the catalyst and the gas. $\theta_{j,p}$ and $R_{j,p}^{het}$ are the coverage and the production rate due to heterogeneous reactions of the j^{th} adsorbed species and σ_{cat} is the concentration of active sites on the catalytic surface.

The evaluation of the catalytic reaction rates is performed by means of the catalyticFOAM framework[6] and they are expressed on the basis of the mean surface molar concentration in the p^{th} particle. Both microkinetic and rate equation models can be adopted for the description of the catalytic chemistry. In case of a microkinetic model, the reaction rates $r_{n,p}$ in the species mass balances are composed by only adsorption and desorption reactions. In case of rate equation kinetics, the site balances are not solved and the reaction rates in the species mass balances represents the kinetics of the whole catalytic process by means of macro-reactions.

According to the hierarchy of the methodology chosen, i.e. Euler-Lagrange CFD-DEM, the gas-particle mass transfer is not quantified directly by means of the indefinite transport equations. Indeed, the computational cells are bigger than particles, thus the gas-particle interface is not described in detail. In this work, the Reichelt correlation[7,8] (Eq. (XI)) have been used to compute the Sherwood Number, from which the gas-particle mass transfer coefficient has been derived.

$$Sh_j = 2 \cdot \frac{\varepsilon}{\tau} + f(\varepsilon) \cdot 0.991 \cdot \left(Re_p Sc_j\right)^{0.33},$$

$$f(\varepsilon) = 1.26 \cdot \left[\frac{1-(1-\varepsilon)^{\frac{5}{3}}}{2-3\cdot(1-\varepsilon)^{\frac{1}{3}}+3\cdot(1-\varepsilon)^{\frac{5}{3}}-2\cdot(1-\varepsilon)^{2}}\right]^{\frac{1}{3}} \tag{XI}$$

where Sc_j is the Schmidt Number related to species *j*.

2.2 Gas Phase

Once the solid phase is updated, the gas-particle momentum and mass transfer contributions are computed for each particle in each cell. By doing so, the interphase momentum and mass source fields are computed and exploited into the gas governing equations (Eqs. (XII)- (XIV)), solved by means of a segregated approach and reported in the following:

$$\frac{\partial(\varepsilon_g \rho_g)}{\partial t} + \nabla \cdot \left(\varepsilon_g \rho_g \boldsymbol{U}_g\right) = 0 \tag{XII}$$

$$\frac{\partial(\varepsilon_g \rho_g \boldsymbol{U}_g)}{\partial t} + \nabla \cdot \left(\varepsilon_g \rho_g \boldsymbol{U}_g \boldsymbol{U}_g\right) = -\varepsilon_g \nabla P - \nabla \cdot \left(\varepsilon_g \bar{\bar{\boldsymbol{\tau}}}\right) + \varepsilon_g \rho_g \boldsymbol{g} + \boldsymbol{S}_U \tag{XIII}$$

$$\frac{\partial(\varepsilon_g \rho_g \omega_{j,g})}{\partial t} + \nabla \cdot \left(\varepsilon_g \rho_g \boldsymbol{U}_g \omega_{j,g}\right) = -\nabla \cdot \left(\varepsilon_g \rho_g \Gamma_j \nabla \omega_{j,g}\right) + R_j^{hom} + \boldsymbol{S}_{\omega_j} \tag{XIV}$$

where $\boldsymbol{U}_g$ is the gas velocity, P is the pressure, **g** is the gravity vector, $\boldsymbol{S}_U$ refers to the gas-solid momentum transfer and $\bar{\bar{\boldsymbol{\tau}}}$ is the Newtonian stress tensor. Γ_j, R_j^{hom} and $\boldsymbol{S}_{\omega_j}$ are the mixture diffusivity, the production rate due to the homogeneous reactions in the gas phase and the gas-solid

mass tranfer of the *j*th species. The evaluation of homogeneous reaction rates is performed by means of openSMOKE++ framework[9]. Nevertheless, they have not been accounted for in this work. The energy balances are implemented in the framework and illustrated in our previous paper[10]. However, they are not herein reported since only isothermal simulations has been performed in this work.

3 References

1 P. Cundall and O. Strack, *Geotechnique*, 1979, **29**, 47–65.
2 Y. Tsuji, T. Tanaka and T. Ishida, *Powder Technol.*, 1992, **71**, 239–250.
3 D. Gidaspow, *Multiphase Flow and Fluidization: Continuum and Kinetic Theory Descriptions*, Academic Press, 1994.
4 H. R. Norouzi, R. Zarghami, R. Sotudeh-Gharebagh and N. Mostoufi, *Coupled CFD-DEM Model. Formul. Implement. Appl. to Multiph. Flows*, 2016, 1–416.
5 L. Naumann and Z. Schiller, *Zeitschrift des Vereines Dtsch. Ingenieure*, 1935, **77**, 318–323.
6 M. Maestri and A. Cuoci, *Chem. Eng. Sci.*, 2013, **96**, 106–117.
7 E. Reichelt, M. Jahn and R. Lange, *Chemie Ing. Tech.*, 2017, **89**, 390–400.
8 F. Scala, *Chem. Eng. Sci.*, 2013, **91**, 90–101.
9 A. Cuoci, A. Frassoldati, T. Faravelli and E. Ranzi, *Comput. Phys. Commun.*, 2015, **192**, 237–264.
10 R. Uglietti, M. Bracconi and M. Maestri, *React. Chem. Eng.*, 2018, **3**, 527–539.